KSCE Journal of Civil Engineering (2020) 24(2):670-681
DOI 10.1007/s12205-019-0996-z

pISSN 1226-7988, eISSN 1976-3808
www.springer.com/12205

Tunnel Engineering

Kinematic Stability of Tunnel Face in Non-Uniform Soils

Jun-Hao Zhong[a] **and Xiao-Li Yang**[a]

[a]*School of Civil Engineering, Central South University, Changsha 410075, China*

ARTICLE HISTORY

Received 3 June 2019
Revised 13 August 2019
Accepted 13 November 2019
Published Online 25 December 2019

KEYWORDS

Stability
Pseudo-dynamic approach
Non-uniform soil
Discretization technique
Earthquakes

ABSTRACT

In the paper, the kinematic analysis is carried out to evaluate the face stability of shallow tunnel in the framework of plasticity theory. In view of the non-uniformity of soil strength parameters, a discretization technique is introduced to generate possible failure mechanisms which respect the associative flow rule and requirement of the non-uniformity of soil strength parameters. As an earthquake situation is considered, a pseudo-dynamic method is adopted to portray the distribution of seismic acceleration. Some comparisons are made to the conventional analysis, including discretization-based pseudo-static analysis and log-spiral-based pseudo-static analysis, to prove the validity of the programming code and accuracy of the proposed method. The soil strength parameters are considered varying in the vertical direction. The effect of distribution of strength parameters is discussed, and distribution form is initially assumed to be linear profile and, then, to be other nonlinear functional profile, including power profile, constant profile and quadratic profile. The results derived from further parametric study show that although the influence of horizontal seismic coefficient is more significant than the vertical one, the vertical effect cannot be ignored in most circumstances, and some factors affect the stability cyclically. In addition, in the linear profile of soil strength parameters, the influence of gradient on supporting pressure is rather small comparing to the average. The influence of non-uniformity of soil strength parameters and seismic parameters on the shape and collapsed area of the failure mechanism is successively studied in this paper. All the optimized solutions are presented in the figures and tables for practical application.

1. Introduction

Geotechnical engineering stability problems have been an important issue of practical engineering for decades. Plenty of works have been implemented in accessing the stability of slopes, retaining structures and tunnel face by the means of limit analysis proposed by Chen (1975). In virtue of the superiority that it can yield an upper or lower bound solution without complicated elastoplastic mechanical analysis, the limit analysis method is widely used in kinematic analysis of geotechnical engineering (Leca and Dormieux, 1990; Mollon et al., 2011; Pan and Dias, 2017; Zhang and Yang, 2019a; 2019b; Li and Yang, 2019b; 2019c; 2020; Huang et al., 2020). By establishing a kinematically admissible velocity field ad statically permissible stress field, the upper and lower bound solution can be calculated readily and the accurate solution is limited in the interval consisting of the upper and lower bound solution.

Many scholars have investigated the stability problems subjected to seepage flow in different ways. In some studies (Michalowski, 1995; Michalowski and Nadukuru, 2013; Li and Yang, 2019a, 2019d; Yang and Zhong, 2019), the effects of pore water pressure as a component of self-gravity are considered by introducing a coefficient r_u initially defined by Bishop and Morgenstern (1960). Perazzelli et al. (2014) adopted a new method to depict the hydraulic head and captured a concise expression from trial and error. It offered some new solutions to the two-dimensional seepage problems of tunnel face. The factor of safety of slope in unsaturated soils is also investigated by Yang and Chen (2019). Besides the effects of underground water, the variation of soil strength parameters is a serious issue as well. Because of the complexity of engineering geological conditions, the actual soil materials are often nonlinear and non-uniform leading to an inconformity to conventional assumptions that soil is linear and uniform. In view of this, Zhang and Yang (2019b) conducted an

CORRESPONDENCE Xiao-Li Yang yangky@aliyun.com School of Civil Engineering, Central South University, Changsha 410075, China

investigation on 3D failure mechanism considering the water. Based on the upper bound theorem of the limit analysis and the tangential technique, both the required reinforcement strength and the stability factor are obtained. The parametric study gives the guidance for designers to choose the better distribution pattern in enhancing the slope.

Except for the unfavorable engineering geological conditions and hydrogeological conditions referred above, the influence of earthquake is also a critical factor for the stability and supposed to be considered in practical engineering. In occurrence of an earthquake, a precise way to describe the seismic effects is taking acceleration time-history as an input, but it might result in a huge computation efforts and time consumption. Thus, a pseudo-static approach comes to be a common choice. Baker et al. (2006) presented a complete design chart for pseudo-static analysis of homogeneous slopes according to a rigorous formulation of the slope stability problem. Some stability charts are offered to evaluate the influences of different parameters on stability for designers. Shukha and Baker (2008) performed a pseudo-static analysis based upon the realization that the direction of the vertical seismic force of a possible earthquake cannot be predicted, so the designers must consider the direction leading to a minimum safety factor. It is emphasized that the influence of vertical seismic force on slope stability is significant in most circumstances, and cannot be neglected. Saada et al. (2013) researched the face stability of a tunnel in terms of the limit analysis upper bound approach in the modified Hoek-Brown geomaterials. A pseudo-static approach is also introduced to access the dynamic effects induced by seismic forces. With the development of technology, the application of mechanized construction is more and more universal in practical engineering presently, which results in a wide use of shield in tunneling projects. More importance had been attached to the face stability to prevent the collapse and ensure the safety. Some scholars (Sahoo and Kumar, 2012; Chakraborty and Kumar, 2013; Sahoo and Kumar, 2014) concentrated on the stability of a long circular tunnel pseudo-static approach.

Although the pseudo-static approach can bring a convenience to the calculation, it neglects the dynamic properties of earthquake. A conservative solution is usually derived. It does not conform to the reality. Thus, a pseudo-dynamic approach is proposed to modify the shortcoming.

Choudhury and Nimbalkar (2007; 2008) investigated the displacement of retaining walls in an earthquake situation by the pseudo-dynamic method considering the active and passive case. Li and Yang (2019d) estimated the active earth pressure for unsaturated soils considering the effect of different water levels, which made research of slope stability even specific and achieve actuality. Additionally, Qin and Chian (2018) presented an original procedure for estimating the ultimate bearing capacity of the soil slopes under earthquake. The seismic acceleration is presented by sine function the pseudo-dynamic method. Since the variation of soil parameters is involved, a discretization technique is used to generate a potential failure mechanism.

However, the pseudo-dynamic analysis focuses on the slopes and retaining structures stability in most existed works and the seismic analysis for tunnels are limited in pseudo-static approach, merely involved in the pseudo-dynamic-based tunnel. To perfect it further, a pseudo-dynamic approach is introduced to the seismic analysis of tunnel face. Combining the variation of soil strength parameters, a discretization technique is used to construct the compatible failure mechanism in this paper. The collapse blocks are sliced into many elements for computing the work rate of external forces. The inertial forces are considered into the equation as an external force which is applied to the soil mass. Distinguished from the conventional pseudo-static analysis, this paper describe the distribution of inertial force by the pseudo-dynamic method, and the vertical seismic acceleration is also considered. Then, according to the limit analysis theorem and virtual work principle, a balanced equation is eventually established. Finally, the least upper bound solution can be derived with the aid of program optimization. The detailed comparison and parametric study are conducted to reveal the influence resulted from the intrinsic dynamic properties of earthquake and variation of soil strength parameters.

2. Methodology

2.1 Pseudo-dynamic Method

The ground motion destructive capacity is closely related to the frequency, amplitude and duration of ground motion. In practical seismic design, a specific parameter is essential to comprehensively reflect various parameters of ground motion. At present, peak ground acceleration (PGA), peak ground velocity (PGV) and peak ground displacement (PGD) indices are commonly used. In China, PGA index is adopted to characterize the ground motion and applied to the Code for Seismic Design of Buildings. Such that is so-called pseudo-static method. However, a rather conservative solution is often derived since the dynamic effect of seismic force, which varies with time and position, is not under consideration. To remedy the deficiencies above, more importance has been attached to employ an appropriate method in presenting dynamic properties of the seismic waves. As for numerical simulation method, a random earthquake input for geotechnical engineering stability analysis is feasible. But the seismic waveforms are too complex to be represented in an exact expression during the theoretical analysis. Thus, the pseudo-dynamic approach comes down to a better alternative.

The seismic waves propagate in the crust and along the surface in the form of the body and surface waves, respectively. The surface waves are often made up of Rayleigh and Love waves which are not considered in this paper. The body waves that propagate in the soil mass include shear and primary waves, and the velocity of which is written as $V_s=\sqrt{G/\rho}$ and $V_p=\sqrt{2G(1-\upsilon)/(\rho(1-2\upsilon))}$, respectively where υ is the Poisson's ratio; G and ρ represent the shear modulus and the density of geomaterials.

An earthquake wave is not only related to the position where

the waves reach to but also is time dependent, thus, it is necessary to introduce the time into the expression of the acceleration. According the seismic wave patterns, the acceleration behaves nearly a cyclic variation. There are several functional forms to describe the regularity of acceleration varying with time among which the trigonometric functions are frequently used. For a real earthquake, each seismic signal can be expressed as a weighted sum of sinusoidal signals based on the Fourier transform. The sine functions are adopted in this paper to further research the influence of initial phase difference between the vertical and horizontal vibrations. Also, the amplification factor f is introduced to portray the effect of magnitude of the seismic acceleration. The factor f which is related to the properties of soil mass materials is assumed as a constant in this paper as the seismic waves propagated from hypocenter to the surface.

With a given amplitude of horizontal and vertical accelerations k_hg and k_vg at the bottom of the tunnel face, the acceleration at random height y_i and time t is presented as:

$$a_h = \left[1+\frac{y_i}{t+H}(f-1)\right]\cdot k_h g\cdot \sin 2\pi\left(\frac{t}{T_s}-\frac{y_i}{\lambda_s}\right) \tag{1}$$

$$a_v = \left[1+\frac{y_i}{t+H}(f-1)\right]\cdot k_v g\cdot \sin 2\pi\left(\frac{t}{T_p}-\frac{y_i}{\lambda_p}+\frac{t_0}{T_p}\right) \tag{2}$$

in which k_h and k_v represent the horizontal and vertical seismic coefficients, and g is the gravity acceleration; T_s and T_p are the periods of the seismic vibration; λ_s and λ_p represent the wavelength and equal T_sV_s and T_pV_p according to the physical relationship, respectively; t_0 is initial phase lag between the horizontal and vertical accelerations at the arch bottom.

2.2 Discretization Technique

The conventional analysis of the face stability is carried out mainly based on translational and rotational failure mechanism whose slip surface is either straight line or logarithmic spiral for uniform cohesive materials. However, the most soil materials are non-homogeneous in nature and the shear strength parameters vary with depth of the overburden and cannot be accounted for easily. Additionally, the classic failure mechanism of tunnel face, log-spiral mechanism (horn shape), is established based on the assumption that geomaterials are uniform. To respect the associative flow rule, the sliding surface should make an angle of φ with the velocity of collapsed blocks. Once the soil is assumed to be non-homogeneous, the log-spiral failure mechanism will be unable to describe the failure model. Therefore, a revised method which encompasses the non-homogeneity of soil is proposed to address above two problems.

In this work, the principal research object is inhomogeneous soil materials. In order to account for the variations of internal friction angle, cohesion and the unit weight of soil mass, a discretized-based method is adopted to generate a new failure mechanism. The discretized technique enables the whole collapsed blocks to be decomposed into infinitesimal quadrilateral elements. It makes the analysis of anisotropic soil mass feasible.

The process of generating the failure mechanism starts from the origin point and ends at the ground surface. With a given point, the adjacent point can be readily determined based on the normality condition which requires angle between the infinitesimal sliding line and velocity vector equal to $\varphi(y_i)$. During the process of tunnel excavation, the active failure resulted from insufficient retaining force is more possible to happen to the face. Hence, the importance will be primarily attached to active failure. The specific procedure for generating the failure mechanism is interrupted later in this paper.

For simplicity, some assumptions are made: 1) the non-uniform soil materials follow the M-C failure criterion; 2) each triangular element rotates around the same point as a rigid body; 3) geomaterials respect the associative flow rule.

3. Generation of Discretization-Based Failure Mechanism

This paper adopted a discretized technique to determine the velocity discontinuous faces of failure mechanism for shallow tunnel. Assuming an active failure, the failure mechanism starts from crown and invert of tunnel face and expand to ground surface which is also bounded by ground surface, discontinuous lines and vertical diameter line, as illustrated in Fig. 1. The main procedure comes down to calculating and locating the points along the sliding surface in turn based on the initial known point.

Initially, two dependent angular variations θ_A and θ_B, and two corresponding initial radius r_A and r_B are defined to determine the position of rotation center. According to the initial conditions and geometric relationship, the coordinates of rotation center O are derived:

$$\begin{cases} r_A = \dfrac{H\cdot\sin\theta_B}{\sin(\theta_A-\theta_B)} \\ r_B = \dfrac{H\cdot\sin(\pi-\theta_A)}{\sin(\theta_A-\theta_B)} \end{cases} \tag{3}$$

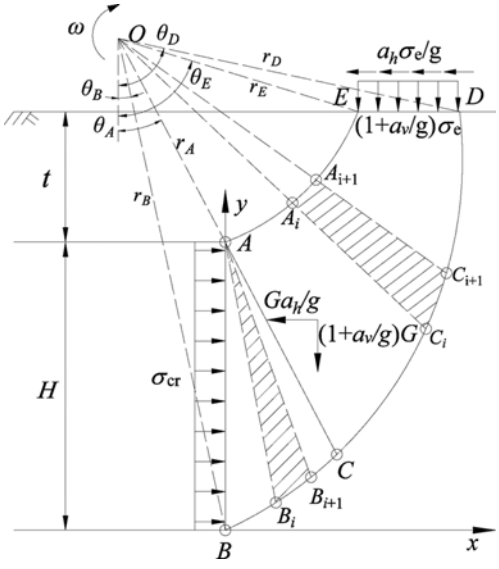

Fig. 1. Schematic Diagram of Generating the Collapsed Mechanism

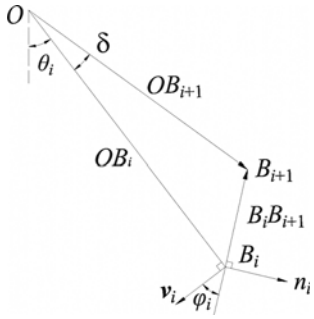

Fig. 2. Determination of the Next Point from a Known Point

$$\begin{cases} x_o = -\dfrac{r_A \cdot r_B \sin(\theta_A - \theta_B)}{H} \\ y_o = \sqrt{r_B^2 - x_o^2} \end{cases} \tag{4}$$

in which H represents the diameter of tunnel.

As shown in Fig. 2, assuming a known random point denoted as $B_i(x_i, y_i)$, the components of unit velocity vector $v_i(v_{xi}, v_{yi})$ at the point B_i can be readily derived based on the normal condition between the prescribed direction of v_i and radial line OB_i:

$$\begin{cases} v_{xi} = -\cos(\theta_i) \\ v_{yi} = -\sin(\theta_i) \end{cases} \tag{5}$$

where θ_i is the angle between the radial line OB_i and the vertical direction. Then, the coordinates of the subsequent point B_{i+1} are determined based on another condition that the unit vector $\boldsymbol{n}_i = (n_{xi}, n_{yi})$ perpendicular to the vector $\boldsymbol{B_iB_{i+1}}$. Meanwhile, the associative flow rule requires the vector $\boldsymbol{v_i}$ to make an angle of $\pi/2+\varphi$ with the unit vector $\boldsymbol{n_i}$, hence, the constraint conditions should be as followed:

$$\begin{cases} \boldsymbol{v}_i \cdot \boldsymbol{n}_i = -\sin\varphi \\ |\boldsymbol{n}_i| = 1 \end{cases} \tag{6}$$

Through conducting algebraic and vector operations to the above simultaneous equation, the following can be deduced:

$$\begin{cases} n_{xi} = \dfrac{-b \pm \sqrt{b^2 - 4ac}}{2a} \\ n_{yi} = \pm\dfrac{\sin\varphi - n_{xi} \cdot \cos\theta_i}{\sin\theta_i} \end{cases} \tag{7}$$

where intermediate quantities a, b, and c read:

$$\begin{cases} a = 1 \\ b = \mp 2\sin\varphi \cdot \cos\theta_i \\ c = \sin^2\varphi - \sin^2\theta_i \end{cases} \tag{8}$$

Substituting OB_{i+1} for the product of λ_{i+1} and unit vector $\boldsymbol{\kappa}_{i+1}$, it gives:

$$\boldsymbol{OB}_{i+1} = \lambda_{i+1} \cdot \boldsymbol{\kappa}_{i+1} \tag{9}$$

where,

$$\boldsymbol{\kappa}_{i+1} = (\sin\theta_{i+1}, -\cos\theta_{i+1}) \tag{10}$$

According to vector operation, $\boldsymbol{B_iB_{i+1}}$ can be further decomposed into:

$$\boldsymbol{B_iB_{i+1}} = \boldsymbol{B_iO} + \boldsymbol{OB}_{i+1} \tag{11}$$

Combining Eqs. (9), (10), and (11), the length of $\boldsymbol{OB}_{i+1}$ is given as:

$$\lambda_{i+1} = \frac{n_{xi}(x_o - x_i) + n_{yi}(y_o - y_i)}{n_{xi}\sin\theta_{i+1} - n_{yi}\cos\theta_{i+1}} \tag{12}$$

Consequently, the coordinates of point B_{i+1} can be ultimately acquired:

$$\begin{cases} x_{i+1} = x_o + \lambda_{i+1}\sin\theta_{i+1} \\ y_{i+1} = y_o - \lambda_{i+1}\cos\theta_{i+1} \end{cases} \tag{13}$$

The procedure elaborated earlier is suitable for the rest of discontinuous faces except for AE, because the angle between the $\boldsymbol{v}_{Ai}$ and $\boldsymbol{n}_{Ai}$ is replaced by $\pi/2 + \varphi$ instead of the formal $\pi/2 + \varphi$. It may induce some difference to the sign of formula which are marked in corresponding equations. The procedure should be repeated for all discretized points by numerical algorithm. As for the shallow tunnels, the collapse mechanism generally protrudes surface. Thus, the points calculated by this algorithm and located on the top of the surface should be deleted. The exact points intersected by the mechanism and surface are calculated by linear interpolation.

The density of the points along the sliding surface depends on the constant angle δ. The smaller δ results in a closer match to the real failure mechanism. The existed work selected a series of δ to plot the failure surfaces, and concluded that a lower δ corresponding to a better solution. Hence, the δ value of 0.01rad in this paper reaches a well compromise between efficiency and results accuracy.

4. Kinematic Stability Analysis

4.1 Conventional Kinematic Analysis

The pseudo-static method is widely used in evaluating seismic stability of geotechnical engineering. It has made a lot of contributions to practical engineering projects for its simplicity and convenience. In this section, a conventional log-spiral-based failure mechanism is employed to analyze the face stability of a circular tunnel. The problems are discussed in uniform geomaterials which are assumed to follow the linear Mohr-Coulomb yield criterion. According to the pseudo static approach, the effects of seismic forces applied to soil mass are considered in the form of vertical and horizontal accelerations which are thought as constants and do not vary with time and position.

Figure 3(b) gives an active failure mechanism with outcrop. It is necessary to consider effect of the surcharge load applied to the failure blocks with a uniform distribution as same as the retaining forces and the seismic forces are often characterized by the earthquake coefficients k_h and k_v. The slip surface is determined by double log-spiral curves whose expressions are presented:

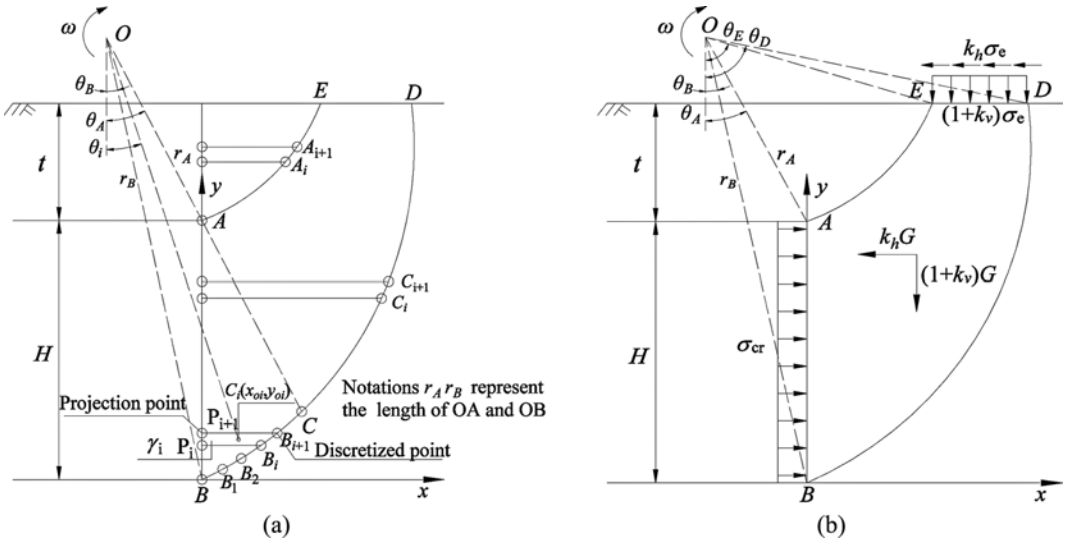

Fig. 3. Schematic Diagram of the Conventional Log-Spiral Mechanism and Discretized Mechanism: (a) Discretized Mechanism, (b) Log-Spiral Mechanism

$$\begin{cases} r_A(\theta) = r_A e^{(\theta-\theta_A)\tan\varphi} \\ r_B(\theta) = r_B e^{(\theta_B-\theta)\tan\varphi} \end{cases} \tag{14}$$

in which θ equals the random rotation angle and φ equals the corresponding friction angle.

In terms of geometric features, the work rate done by soil gravity and inertial forces can be calculated by integrating, yielding:

$$\begin{aligned} \dot{W}_\gamma = {} & (1+k_v)\left(\gamma\omega r_B^3 f_3 - \gamma\omega r_A^3 f_4 - \gamma\omega r_A^3 f_5 - \gamma\omega r_A^3 f_1\right) \\ & + k_h\left(\gamma\omega r_B^3 f_3' - \gamma\omega r_A^3 f_4' - \gamma\omega r_A^3 f_5' - \gamma\omega r_A^3 f_1'\right) \end{aligned} \tag{15}$$

where $f_i(i=1,2\ldots)$ represents the dimensionless functions, which are given in detail in appendix. Similarly, the work rate done by surcharge load and inertial forces is given as:

$$\dot{W}_e = (1+k_v)\sigma_e\omega r_A^2 f_6 + k_h\sigma_e\omega r_A^2 f_6' \tag{16}$$

The work rate of retaining forces is given as:

$$\dot{W}_{cr} = \sigma_{cr}\omega r_B^2 f_2 \tag{17}$$

Due to the seismic inertial forces having no impact on the energy dissipation rate, the power dissipated on the sliding surface is yielded as:

$$\dot{W}_D = c\omega r_B^2 f_7 + c\omega r_A^2 f_8 \tag{18}$$

According to the power balance equation, the expression of retaining force in the limit state is eventually derived as:

$$\sigma_{cr} = \frac{\dot{W}_D - \dot{W}_\gamma - \dot{W}_e}{r_B^2 f_2} \tag{19}$$

4.2 Discretized-Based Kinematic Analysis

According to the failure mechanism interrupted in previous section, it can be obtained that the discontinuous lines consist of discretized points by which the entire collapsed block is decomposed into infinitesimal elements and the dynamic acceleration is able to be incorporated into the analysis. Due to the soil strength parameters varying with the depth, the triangular element used to locate the adjacent point is not appropriate again to calculate the work rate done by external forces, and another trapezoidal element is introduced to the kinematic analysis. Given two initial adjacent points from which the radial lines extend horizontally, other two points intersected at tunnel face are derived. The trapezoidal element is formed by connecting the four points.

For instance, a random trapezoidal element, $B_iB_{i+1}P_iP_{i+1}$ with P_i and P_{i+1} being the projections of B_i and B_{i+1}, as shown in Fig. 3(a), is chosen to demonstrate the procedure of computing the work rate. According to coordinate system that takes B as origin point, the area of the trapezoidal element yields:

$$A_i = \frac{1}{2}\left(x_i - y_i + x_{i+1} - y_{i+1}\right)\left(y_{i+1} - y_i\right) \tag{20}$$

The gravity center of the ith element is denoted as $C_i(x_{oi},y_{oi})$ and the external forces including soil gravity, seismic forces and surcharge, are closely related to the linear velocity of point C_i. According to the geometric features of the ith element, the coordinates of centroid are given as:

$$x_{oi} = \frac{x_i \cdot x_i + x_{i+1}\left(x_i + x_{i+1}\right)}{3\left(x_i + x_{i+1}\right)} \tag{21}$$

$$y_{oi} = \frac{x_i\left(2y_i + y_{i+1}\right) + x_{i+1}\left(y_i + 2y_{i+1}\right)}{3\left(x_i + x_{i+1}\right)} \tag{22}$$

The length of v_i is presented as:

$$v_i = \omega\sqrt{\left(x_o - x_{oi}\right)^2 + \left(y_o - y_{oi}\right)^2} \tag{23}$$

in which ω equals the angular velocity at failure. Based on the

definition of power, the total work rate produced by collapsed blocks weight for entire elements give:

$$\dot{W}_G = \sum_i \gamma_i A_i \omega \sqrt{(x_o - x_{oi})^2 + (y_o - y_{oi})^2} \sin\theta_{Gi} \tag{24}$$

where γ_i equals unit weight of soil for the ith element, and θ_{Gi} represents the angle between the vertical direction and the ith radial line passing through the gravity center, as shown in Fig. 3(a).

Similarly, the work rates of horizontal and vertical inertia forces induced by earthquake acting on the ith element yield:

$$\dot{W}_{Gh} = \sum_i \gamma_i A_i \omega \sqrt{(x_o - x_{oi})^2 + (y_o - y_{oi})^2} \cos\theta_{Gi} \left[1 + \frac{y_i}{t+H}(f-1)\right] k_h \sin 2\pi \left(\frac{t}{T_s} - \frac{y_i}{\lambda_s}\right) \tag{25}$$

$$\dot{W}_{Gv} = \sum_i \gamma_i A_i \omega \sqrt{(x_o - x_{oi})^2 + (y_o - y_{oi})^2} \sin\theta_{Gi} \left[1 + \frac{y_i}{t+H}(f-1)\right] k_v \sin 2\pi \left(\frac{t}{T_p} - \frac{y_i}{\lambda_p} + \frac{t_0}{T_p}\right) \tag{26}$$

In the case of collapsed mechanism expanded to ground surface for shallow tunnels, it is necessary to consider the surcharge which is generally assumed as uniform distribution. The ground motion can be regarded as free vibration while the seismic waves propagate to the ground surface, and expression of the horizontal and vertical acceleration is degenerated into:

$$a_{eh} = f k_h g \cdot \sin 2\pi \left(\frac{t}{T_s} - \frac{y_i}{\lambda_s}\right) \tag{27}$$

$$a_{ev} = f k_v g \cdot \sin 2\pi \left(\frac{t}{T_p} - \frac{y_i}{\lambda_p} + \frac{t_0}{T_p}\right) \tag{28}$$

The work rates done by surcharge load can be calculated by following formula, as illustrated in Fig. 4.

$$\dot{W}_e = \int_{\theta_E}^{\theta_D} \sigma_e v \cdot \sin\theta \, d\theta \tag{29}$$

The work rate incorporating in horizontal and vertical inertia forces of surcharge can be eventually expressed as:

$$\dot{W}_{eh} = \sigma_e \left(r_D \sin\theta_D - r_E \sin\theta_E\right) f k_h \cdot \sin 2\pi \left(\frac{t}{T_s} - \frac{y_i}{\lambda_s}\right) \cdot \omega \left(y_O - \frac{h_e}{2} - y_D\right) \tag{30}$$

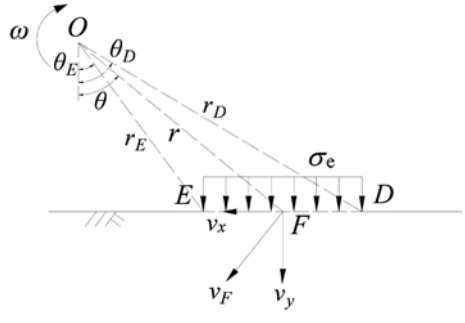

Fig. 4. Calculation of the Work Rates Done by Surcharge Load

$$\dot{W}_{ev} = \sigma_e \left(r_D \sin\theta_D - r_E \sin\theta_E\right) f k_v \cdot \sin 2\pi \left(\frac{t}{T_p} - \frac{y_i}{\lambda_p} + \frac{t_0}{T_p}\right) \cdot \omega \left(\frac{x_D - x_E}{2} - x_O\right) \tag{31}$$

As the active failure happened, the collapsed blocks rotate around the rotation center with an angular velocity. The shear stress along the slip surface, that is the sole resistance, induces the energy consumption through the plastic deformation. For the ith element, the energy dissipated along the sliding surface can be expressed by the dot product of cohesion and velocity vector and it yields:

$$D_i = c_i L_i \cdot \omega R_i \cos\varphi_i \tag{32}$$

in which L_i and R_i equal the length of B_iB_{i+1} and distance from rotation center to the ith discretized point, respectively. The detailed expressions are given as:

$$L_i = \sqrt{(x_{i+1} - x_i)^2 + (y_{i+1} - y_i)^2} \tag{33}$$

$$R_i = \sqrt{(x_i - x_o)^2 + (y_i - y_o)^2} \tag{34}$$

The total rate of internal energy dissipation can be attained by summarizing all elementary dissipation rates along the slip surface, and it yields:

$$D = \sum_i c_i L_i \cdot \omega R_i \cos\varphi_i \tag{35}$$

The procedure elaborated above gives a discretization-based kinematic analysis the seismic face stability by the means of pseudo-dynamic approach. The upper bound solution expressed as the objective function $\sigma_{cr} = f(\theta_A, \theta_B, t/T)$ can be derived from the equilibrium of total external work rate and the internal energy dissipation. With the help of computer programming, the least solution can be obtained by optimizing the variables of objective function based on the given parameters.

5. Comparison and Discussion

5.1 Comparison

It can be noted that the horizontal and vertical pseudo-dynamic accelerations are degraded into the k_hg and k_vg while time and position variables are removed from the acceleration expression and the soil amplification, namely f, is set to 1.0. Then, the pseudo-dynamic approach is converted to pseudo-static approach. Therefore, the corresponding pseudo-static solution can be readily derived by optimizing the variables of objective function $\sigma_{cr} = f(\theta_A, \theta_B)$. In order to further prove rationality of the pseudo-dynamic approach and the validity of program algorithm, results calculated by different methods are presented in this section for comparison. According to basic inputted parameters: $C = 4$ m, $d = 10$ m, $c_0 = c_h = 10$ kpa, $\varphi_0 = \varphi_h = 15^\circ$, $\gamma_0 = \gamma_h = 18$ kN/m^2, $k_h = 0.2$, $u_v = 0.5$, $T = 0.2s$; $t_0/T = 0$; $\sigma_e = 10$ kPa; $G = 200$ MPa and $\upsilon = 0.3$, the comparative results are listed in Tables 1 – 2.

It can be noticed that the pseudo-static solutions are greater than pseudo-dynamic solutions, but the difference is not significant,

Table 1. Comparison of Supporting Pressure in Different Failure Mechanism and Seismic Analysis

φ	Pseudo-static approach						Pseudo-dynamic approach			Maximum difference (%)
	Discretized mechanism			Log-spiral mechanism			Discretized mechanism			
	$c = 10$	$c = 15$	$c = 20$	$c = 10$	$c = 15$	$c = 20$	$c = 10$	$c = 15$	$c = 20$	
5	282.83	252.43	224.44	279.91	249.81	222.10	282.12	251.75	223.81	1.04
10	186.08	169.41	153.51	184.35	167.70	151.84	185.77	169.13	153.24	0.94
15	137.86	124.32	110.96	136.40	122.91	109.60	137.69	124.16	110.81	1.07
20	102.11	90.18	78.32	100.89	89.01	77.20	102.01	90.09	78.22	1.21
25	73.87	63.23	52.62	72.87	62.28	51.72	73.81	63.17	52.56	1.37

Table 2. Comparison of Pseudo-static and Pseudo-dynamic Solutions in Supporting Pressure

φ	Pseudo-static approach						Pseudo-dynamic approach			Maximum difference (%)
	Discretized mechanism			Log-spiral mechanism			Discretized mechanism			
	$k_h = 0.1$	$k_h = 0.3$	$k_h = 0.5$	$k_h = 0.1$	$k_h = 0.3$	$k_h = 0.5$	$k_h = 0.1$	$k_h = 0.3$	$k_h = 0.5$	
5	139.82	194.73	282.83	140.00	192.63	279.91	139.8	194.36	282.12	0.14
10	107.61	142.69	186.08	106.19	141.13	184.35	107.59	142.55	185.77	1.34
15	80.83	107.81	137.86	79.92	106.51	136.40	80.80	107.72	137.69	1.14
20	58.19	79.46	102.11	57.26	78.39	100.89	58.18	79.40	102.01	1.62
25	39.22	56.20	73.87	38.48	55.33	72.87	39.21	56.16	73.81	1.92

because pseudo-dynamic acceleration is assumed as sine waves whose amplitude is yet taken as the value of acceleration in pseudo-static approach and its value is up to maximum at point of invert when time t is set as $T/4$. Besides, the wavelength is far greater than the distance from invert of tunnel to surface which causes the variation of acceleration to be small enough and results in an insignificant difference. The correctness of the proposed method is proved and also indirectly reflected that the pseudo-static approach is conservative.

5.2 Parametric Studies

As elaborated earlier, the critical supporting pressure is a function of initial angles θ_A, θ_B and t/T. The face stability is associated with a series of parameters which reflect the non-uniformity of soil strength and intrinsic dynamic properties of earthquakes. Therefore, a parametric analysis is conducted to study the influence of each parameter variables in this section. The optimized results are given with following basic parameters: c_0 = 10 kPa, c_h = 20 kPa, $\varphi_0 = 15^o$, $\varphi_h = 25^o$, γ_0 = 16 kN/m^3, γ_h = 22 kN/m^3, $k_h = 0.5$, $u_v = 0.5$, $T = 0.2$s, $t_0/T = 0$, $f = 1$, σ_e = 10 kPa, t = 4 m and H = 10 m.

With k_h being a constant, the variation trend of retaining force applied to the tunnel face is presented in Fig. 5 where surcharge loads range from 0 to 40 kPa at an interval of 10 kPa. It shows that the retaining force increases with a higher value of horizontal seismic coefficient, and the increment of retaining force exceeds over 50% as k_h ranges from 0 to 0.5, which indicates that the effect of horizontal seismic coefficient is sensitive. It also implies that the surcharge load is an unfavorable factor for the stability of tunnel face whose effect is approximately proportional to the value of surcharge.

Apart from the horizontal seismic coefficient, the vertical

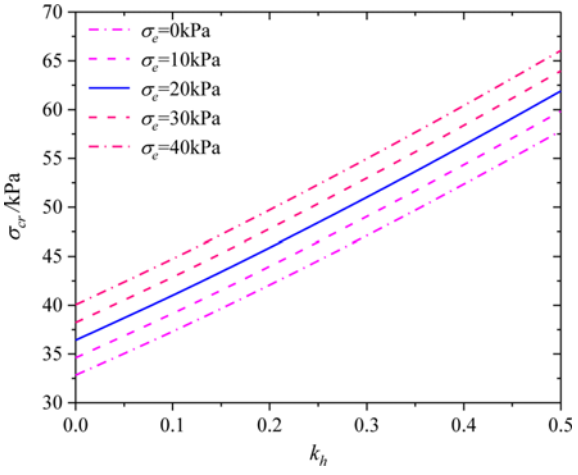

Fig. 5. Supporting Pressure under Different Horizontal Seismic Coefficient and Surcharge

seismic coefficient also influences the critical supporting pressure. The relationship between μ_v ratio and critical supporting force is presented in Fig. 6 where a higher value of μ_v causes a larger requirement of retaining force, and the increment of supporting pressure is no more than 20% while μ_v varies from 0 to 1. The insignificant difference maybe the reason why the vertical seismic wave is merely considered in the most seismic analysis.

For portraying the variation in magnitude of seismic acceleration, the factor f is introduced to present the magnitude as seismic waves propagating to the surface. The results given in Fig. 7 indicate that the face stability decreases directly and retaining force increases synchronously when soil amplification factor ranges from 1 to 2. The trend of supporting pressure behaves

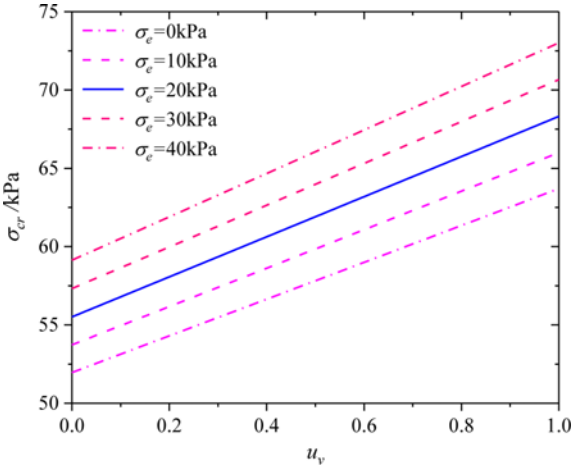

Fig. 6. Supporting Pressure under Different Vertical Seismic Coefficient and Surcharge

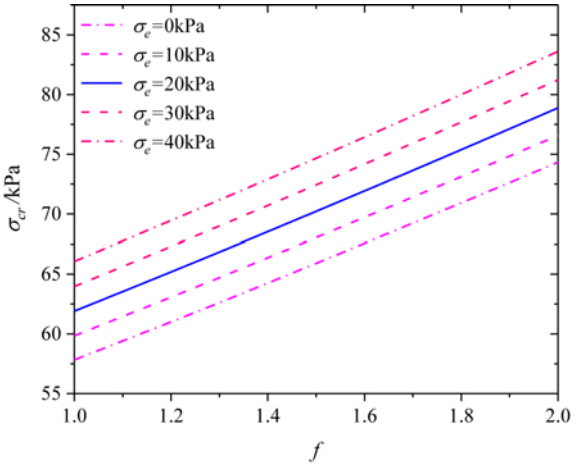

Fig. 7. Effect of Soil Amplification Factor and Surcharge on Supporting Pressure

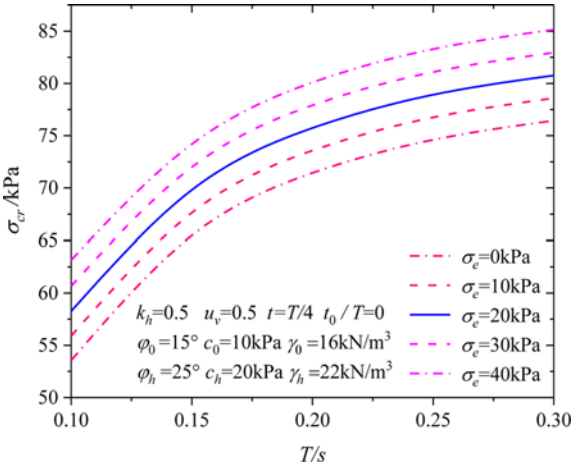

Fig. 8. Effect of Vibration Period and Surcharge on Supporting Pressure

closer to be linear. Apart from the effects of soil amplification factor and seismic coefficients, the period and phase shifts to some extent influence the stability of tunnel face.

When the time is fixed at T/4, the seismic wave is a function

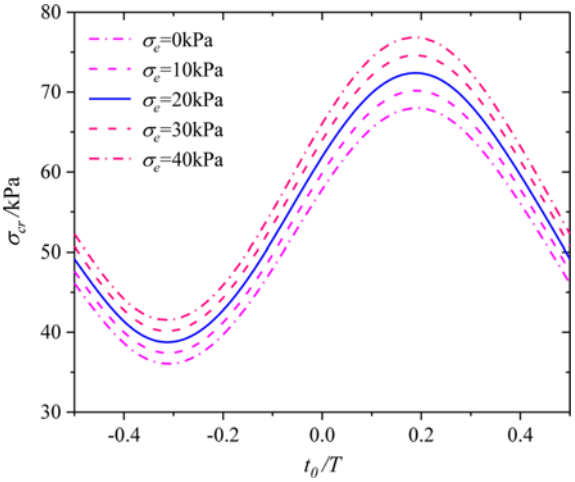

Fig. 9. Effect of Initial Phase Shift and Surcharge on Supporting Pressure

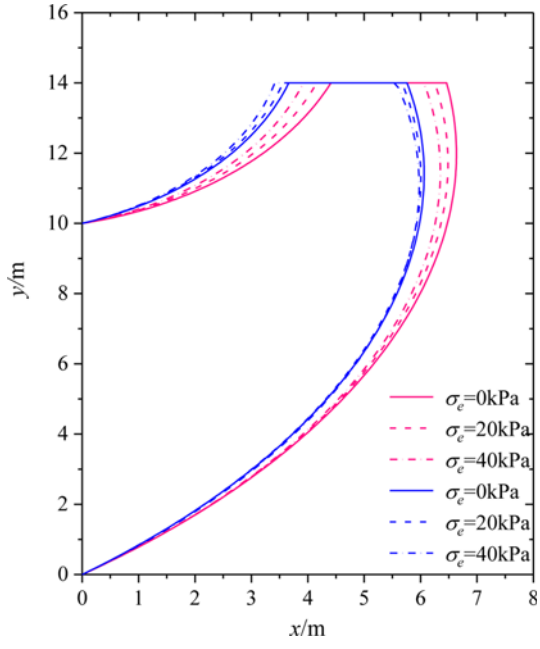

Fig. 10. Effect of Horizontal Seismic Coefficient and Surcharge on Failure Mechanism

of position solely. At this time, the shape of seismic waves is closely related to the period T which directly affects the distribution of seismic acceleration. Fig. 8 performs a further investigation of the influence of period T, and implies that an increase in period leads to an increment of retaining force in a non-linear way. It is because the values of sine waves alternate in the positive and negative regions, which might cause an offset in the rate of inertial force. If a period approaches to the infinite, the seismic acceleration will be approximately equal to amplitude. As seismic waves propagating from the invert of tunnel face to the surface, a phase shift inevitably exists. To figure out the intrinsic influence of phase shift, Fig. 9 portrays a series of curves with t_0/T range in $[-1/2,1/2]$. According to feature of curves, it can be found that the results experience a whole sine wave in a completed period and return to the initial value in the end. The

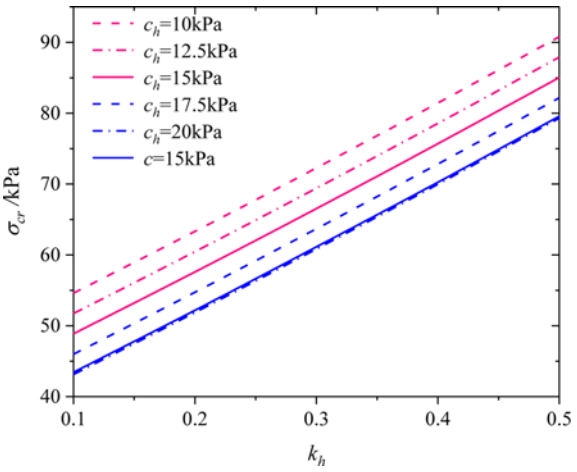

Fig. 11. Effect of Non-Uniform Distribution of c on Supporting Pressure

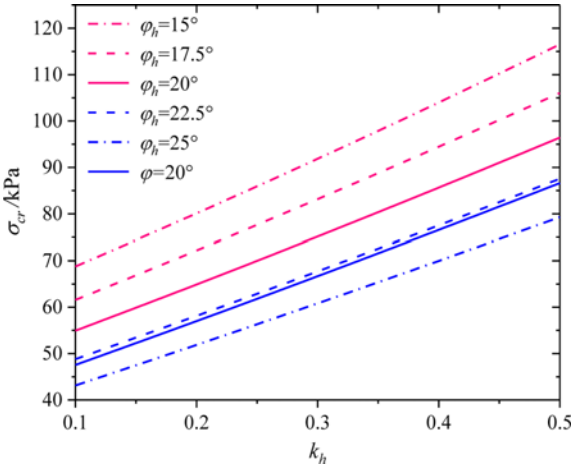

Fig. 12. Effect of Non-Uniform Distribution of φ on Supporting Pressure

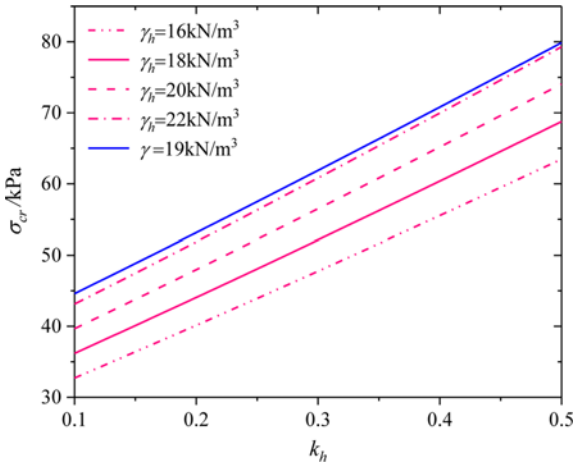

Fig. 13. Effect of Non-Uniform Distribution of γ on Supporting Pressure

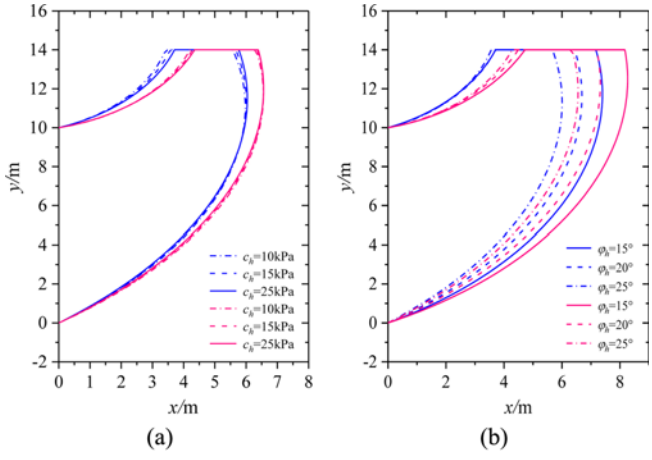

Fig. 14. Effect of Various Gradient for Soil Strength Parameters on Failure Mechanism under Linear Profile: (a) For Cohesion, (b) For Internal Friction Angle

whole process is regular and behaves a cyclic characteristic because of the dynamic properties of earthquake.

Figure 10 gives a series of potential failure mechanisms under different surcharge loading to investigate the influence of horizontal seismic coefficient on the shape of collapsed mechanism. The red lines and blue lines represent cases that k_h equals 0.3 and 0.5, respectively. It shows that the mechanisms tend to move away from the tunnel face and failure areas expand in higher value of surcharge while k_h is kept as a constant.

Assuming that the soil strength parameters distribute in the form of linearity from the ground surface to the bottom of tunnel, Figs. 11 analyzes the effect of non-homogeneity of cohesion. With a proper given initial value on ground surface, the results of linear profile in different inclination degree can be obtained by assigning various values to c_h. It could be observed that a larger c_h results in a small retaining force. It is worth noticing that the difference between the average cohesion and c_h = 20 kPa is very small.

Similarly, the influence of parameters φ_h and γ_h are investigated in the same way. However, as shown in Fig. 12, the results of φ = 20° are close to the results of φ_h = 22.5° which differs from the influence of parameter c_h. In Fig. 13, the retaining force increases with the increase of unit weight of soil with γ_h ranging from 16 to 22 kN/m³ and an average γ of 19 kN/m³ yields a maximum of retaining force.

The inhomogeneity of soil strength parameters not only influences the face stability but also affects shape of failure mechanism. Fig. 14 mainly studies the impact on failure mechanism about different gradient of linear function. Comparing to the cohesion, the friction angle seems to have a greater influence on the shape mechanism. The red one (k_h = 0.5) leads to a larger distance forward than the blue one (k_h = 0.3), which indicates the influence of seismic coefficient in the dominance. As for friction angle, the advanced displacement of the right slip surface is obviously larger than the left one.

Except for the linear distribution, the effects of other different functional profiles of soil strength parameters are also researched, including linear function, quadratic function and power function.

Out of the four kinds of profile of soil strength parameters, the quadratic and power profiles derive the minimum and maximum, respectively. This is because the quadratic profile provides the

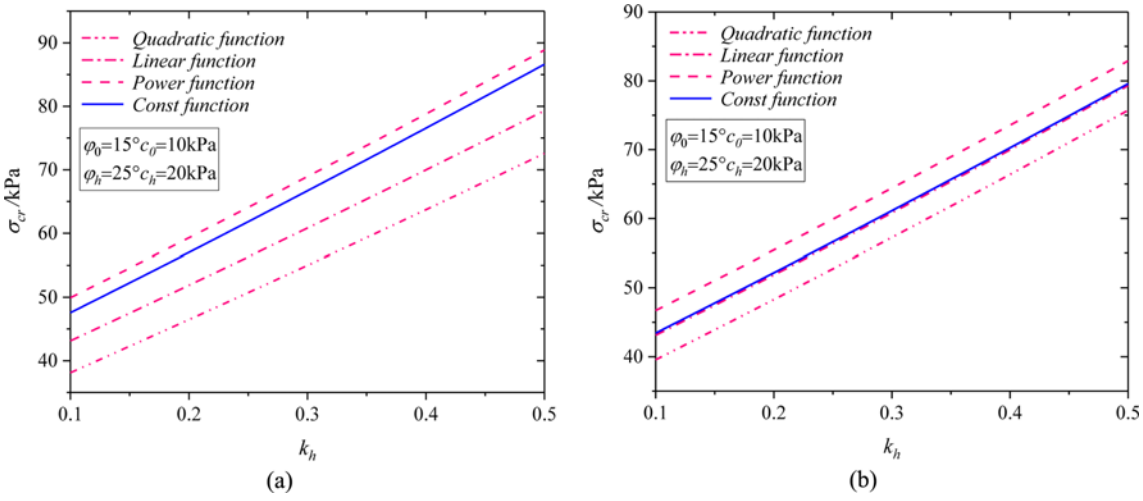

Fig. 15. Effect of Various Functional Profiles for c and φ on Supporting Pressure: (a) For Cohesion, (b) For Internal Friction Angle

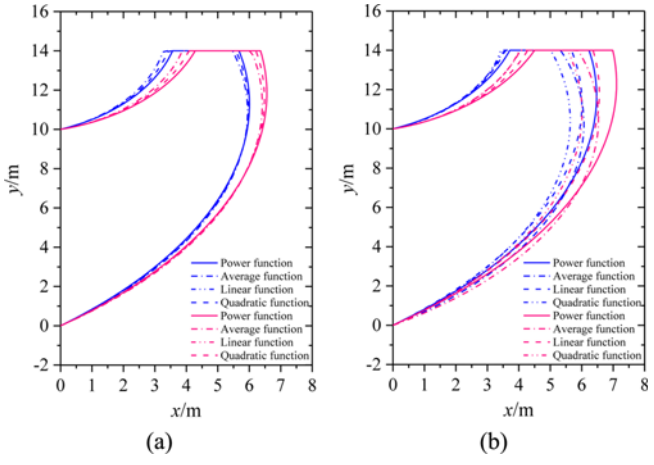

Fig. 16. Effect of Various Functional Profile for Soil Strength Parameters on Failure Mechanism: (a) For Cohesion, (b) For Internal Friction Angle

least resistance to the soil but the power profile provides biggest resistance overall. The constant profile results in a smaller result following the results of the power profile, because the power profile provides a smaller soil strength to stability.

The results presented in Fig. 16 imply that the largest collapsed area is induced by power function profile, because the power function profile provides the least soil strength parameters, thus, the tunnel needs a bigger retaining force to sustain the stability. The strength provided by quadratic function profile is larger than other three cases, therefore, a greater collapsed area is provoked.

6. Conclusions

In this work, a new procedure is proposed to evaluate the face stability of a shallow tunnel in virtue of limit analysis upper bound method. To account for the effects of the non-uniform soil strength parameters, a discretized technique is adopted to disperse the slip surface into a series of points and to generate a compatible failure mechanism in the non-uniform soils. By utilizing the pseudo-dynamic approach, an earthquake situation is also considered and the intrinsic dynamic properties of earthquake are better reflected. Apart from the pseudo-dynamic analysis, the pseudo-static analysis is also presented to prove the validity of proposed method. Some comparisons are made between discretization-based pseudo-static analysis, discretization-based pseudo-dynamic analysis and log-spiral-based pseudo-static analysis, and the comparative results verify the correctness of the programming code and accuracy of the proposed method.

Due to the diversity of distribution of soil strength parameters, the soil strength parameters maybe distributed in any forms. In the circumstance that the soil materials distributed in the form of linear function from surface to underground, the effect of different gradient of linear function is of importance and necessary to be investigated in detail. Apart from the linear case, four other kinds of functional profile, including power profile, constant profile and quadratic profile are further studied and all the optimized results are shown in the figures. On the basis of assumptions of various functional profile above, the influence of non-uniformity of soil strength parameters and seismic parameters on the shape and collapsed area of the failure mechanism is plotted in this paper in turn.

It is necessary to emphasize that the optimized upper bound solutions is smaller than conventional analysis, indicating that the existed solutions are conservative, and the proposed method is closer to real solution. The following conclusions can be summarized:

1. According to basic inputted parameters, when a random time is fixed as $T/4$, the difference between pseudo-dynamic approach and pseudo-static approach is rather small in both discretization-based mechanism and log-spiral mechanism.
2. The vertical and horizontal seismic coefficients are unfavorable factors for the face stability, and the horizontal seismic coefficient is more sensitive. Conversely, a longer period is adverse to the face stability. The influence of phase shift is

sine curve which is cyclic characteristic.

3. Different functional models of distribution of soil strength parameters influence the retaining force differently; power function profile affects it most prominently, followed by linear profile and quadratic profile. The influence of average profile is the same as linear profile.
4. As for failure mechanism, it tends to move away from the tunnel face as influential factors result in a significant demand of retaining force.

Acknowledgements

Not Applicable

ORCID

Not Applicable

References

Baker R, Shukha R, Operstein V, Frydman S (2006) Stability charts for pseudo-static slope stability analysis. *Soil Dynamics and Earthquake Engineering* 26(9):813-823, DOI: 10.1016/j.soildyn.2006.01.023

Bishop AW, Morgenstern NR (1960) Stability coefficients for earth slopes. *Geotechnique* 10(4):129-150, DOI: 10.1680/geot.1960.10.4.129

Chakraborty D, Kumar J (2013) Stability of a long unsupported circular tunnel in soils with seismic forces. *Natural Hazards* 68(2):419-431, DOI: 10.1007/s11069-013-0633-y

Chen WF (1975) Limit analysis and soil plasticity. Elsevier Science, Amsterdam, Netherlands DOI: 10.2136/sssaj1976.03615995004000040002x

Choudhury D, Nimbalkar S (2007) Seismic rotational displacement of gravity walls by pseudo-dynamic method: Passive case. *Soil Dynamics and Earthquake Engineering* 27(3):242-249, DOI: 10.1016/j.soildyn.2006.06.009

Choudhury D, Nimbalkar S (2008) Seismic rotational displacement of gravity walls by pseudodynamic method. *International Journal of Geomechanics* 8(3):169-175, DOI: 10.1061/(ASCE)1532-3641

Huang F, Zhang M, Wang F, Ling TH, Yang XL (2020) The failure mechanism of surrounding rock around an existing shield tunnel induced by an adjacent excavation. *Computers and Geotechnics* 117:103236, DOI: 10.1016/j.compgeo.2019.103236

Leca E, Dormieux L (1990) Upper and lower bound solutions for the face stability of shallow circular tunnels in frictional material. *Geotechnique* 40(4):581-606, DOI: 10.1680/geot.1990.40.4.581

Li YX, Yang XL (2019a) Seismic displacement of 3D slope reinforced by piles with nonlinear failure criterion. *International Journal of Geomechanics* 19(6):04019042, DOI: 10.1061/(ASCE)GM.1943-5622.0001411

Li TZ, Yang XL (2019b) Probabilistic analysis for face stability of tunnels in Hoek-Brown media. *Geomechanics and Engineering* 18(6):595-603, DOI: 10.12989/gae.2019.18.6.595

Li TZ, Yang XL (2019c) Face stability analysis of rock tunnels under water table using Hoek-Brown failure criterion. *Geomechanics and Engineering* 18(3):235-245, DOI: 10.12989/gae.2019.18.3.235

Li ZW, Yang XL (2019d) Active earth pressure from unsaturated soils with different water levels. *International Journal of Geomechanics* 19(7):06019013, DOI: 10.1061/(ASCE)GM.1943-5622.0001471

Li TZ, Yang XL (2020) Stability of plane strain tunnel headings in soils with tensile strength cut-off. *Tunnelling and Underground Space Technology* 95:103138, DOI: 10.1016/j.tust.2019.103138

Michalowski RL (1995) Slope stability analysis: A kinematical approach. *Geotechnique* 45(2):283-293, DOI: 10.1680/geot.1995.45.2.283

Michalowski RL, Nadukuru SS (2013) Three-dimensional limit analysis of slopes with pore pressure. *Journal of Geotechnical and Geoenvironmental Engineering* 39(9):1604-1610, DOI: 10.1061/(ASCE)GT.1943-5606.0000867

Mollon G, Phoon KK, Dias D, Soubra AH (2011) Validation of a new 2D failure mechanism for the stability analysis of a pressurized tunnel face in a spatially varying sand. *Journal of Engineering Mechanics* 137(1):8-21, DOI: 10.1061/(ASCE)EM.1943-7889.0000196

Pan QJ, Dias D (2017) Upper-bound analysis on the face stability of a non-circular tunnel. *Tunnelling and Underground Space Technology* 62:96-102, DOI: 10.1016/j.tust.2016.11.010

Perazzelli P, Leone T, Anagnostou G (2014) Tunnel face stability under seepage flow conditions. *Tunnelling and Underground Space Technology* 43:459-469, DOI: 10.1016/j.tust.2014.03.001

Qin CB, Chian SC (2018) Seismic bearing capacity of non-uniform soil slopes using discretization-based kinematic analysis considering rayleigh waves. *Soil Dynamics and Earthquake Engineering* 109:23-32, DOI: 10.1016/j.soildyn.2018.02.017

Saada Z, Maghous S, Garnier D (2013) Pseudo-static analysis of tunnel face stability using the generalized hoek-brown strength criterion. *International Journal for Numerical and Analytical Methods in Geomechanics* 37(18):3194-3212, DOI: 10.1002/nag.2185

Sahoo JP, Kumar J (2012) Seismic stability of a long unsupported circular tunnel. *Computers and Geotechnics* 44:109-115, DOI: 10.1016/j.compgeo.2012.03.015

Sahoo JP, Kumar J (2014) Stability of a circular tunnel in presence of pseudostatic seismic body forces. *Tunnelling and Underground Space Technology* 42:264-276, DOI: 10.1016/j.tust.2014.03.003

Shukha R, Baker R (2008) Design implications of the vertical pseudo-static coefficient in slope analysis. *Computers and Geotechnics* 35(1):86-96, DOI: 10.1016/j.compgeo.2007.01.005

Yang XL, Chen JH (2019) Factor of safety of geosynthetic-reinforced slope in unsaturated soils. *International Journal of Geomechanics* 19(6):04019041, DOI: 10.1061/(ASCE)GM.1943-5622.0001399

Yang XL, Zhong JH (2019) Stability analysis of tunnel face in nonlinear soil under seepage flow. *KSCE Journal of Civil Engineering* 23(9):4553-4563, DOI: 10.1007/s12205-019-0601-5

Zhang R, Yang XL (2019a) New 3D failure analysis of water-filled karst cave beneath deep tunnel. *Geomechanics and Engineering* 18(1):1-9, DOI: 10.12989/gae.2019.18.1.001

Zhang R, Yang XL (2019b) Limit analysis of anchor trapdoor embedded in nonhomogeneous and nonlinear soils. *International Journal of Geomechanics* 19(8):04019089, DOI: 10.1061/(ASCE)GM.1943-5622.0001476

Appendix

$$f_1(\theta_A,\theta_B)=\frac{\sin^2\theta_A\cdot\sin(\theta_A-\theta_B)}{3\sin\theta_B} \tag{36}$$

$$f_1'(\theta_A,\theta_B)=\frac{\sin\theta_A\cdot\sin(\theta_A-\theta_B)\sin(\theta_A+\theta_B)}{6\sin^2\theta_B} \tag{37}$$

$$f_2(\theta_A,\theta_B)=\frac{1}{2}\left(\frac{\sin^2\theta_B}{\sin^2\theta_A}-1\right) \tag{38}$$

$$f_3(\theta_B,\theta_D)=\frac{3\tan\varphi\sin\theta_B+\cos\theta_B-(3\tan\varphi\sin\theta_D+\cos\theta_D)\exp\left[3\tan\varphi(\theta_B-\theta_D)\right]}{3\left(1+9\tan^2\varphi\right)} \tag{39}$$

$$f_3^{'}(\theta_B,\theta_D)=\frac{3\tan\varphi\cos\theta_B-\sin\theta_B-(3\tan\varphi\cos\theta_D-\sin\theta_D)\exp\left[3\tan\varphi(\theta_B-\theta_D)\right]}{3\left(1+9\tan^2\varphi\right)} \tag{40}$$

$$f_4(\theta_A,\theta_B,\theta_D,\theta_E)=\frac{\sin(\theta_D-\theta_E)\sin\theta_D\sin^2\theta_A\exp\left[\tan\varphi(2\theta_B-2\theta_D+\theta_E-\theta_A)\right]}{6\sin^2\theta_B}+\frac{\sin(\theta_D-\theta_E)\sin\theta_E\sin\theta_A\exp\left[\tan\varphi(\theta_B-\theta_D+2\theta_E-2\theta_A)\right]}{6\sin\theta_B} \tag{41}$$

$$f_4^{'}(\theta_A,\theta_D,\theta_E)=\frac{\sin(\theta_D-\theta_E)\cos^2\theta_E\exp\left[3\tan\varphi(\theta_E-\theta_A)\right]}{3\cos\theta_D} \tag{42}$$

$$f_5(\theta_A,\theta_E)=\frac{(3\tan\varphi\sin\theta_E-\cos\theta_E)\exp\left[3\tan\varphi(\theta_E-\theta_A)\right]-3\tan\varphi\sin\theta_A+\cos\theta_A}{3\left(1+9\tan^2\varphi\right)} \tag{43}$$

$$f_5^{'}(\theta_A,\theta_E)=\frac{(3\tan\varphi\cos\theta_E+\sin\theta_E)\exp\left[3\tan\varphi(\theta_E-\theta_A)\right]-(3\tan\varphi\cos\theta_A+\sin\theta_A)}{3\left(1+9\tan^2\varphi\right)} \tag{44}$$

$$f_6(\theta_A,\theta_D,\theta_E)=\frac{1}{2}\exp\left[2\tan\varphi(\theta_E-\theta_A)\right]\left(\frac{\cos^2\theta_E}{\cos^2\theta_D}-1\right) \tag{45}$$

$$f_6^{'}(\theta_A,\theta_D,\theta_E)=\frac{\exp\left[2\tan\varphi(\theta_E-\theta_A)\right]\sin(\theta_D-\theta_E)\cos\theta_E}{\cos\theta_D} \tag{46}$$

$$f_7(\theta_B,\theta_D)=\frac{1-\exp\left[2\tan\varphi(\theta_B-\theta_D)\right]}{2\tan\varphi} \tag{47}$$

$$f_8(\theta_A,\theta_E)=\frac{\exp\left[2\tan\varphi(\theta_E-\theta_A)\right]-1}{2\tan\varphi} \tag{48}$$